공학석사학위논문

Electron Heat Transport Study in KSTAR L-mode Plasmas Using ECRH Modulation

KSTAR L-모드 플라즈마에서 ECRH 모듈레이션을 이용한 전자 열 수송 연구

2018년 2월

서울대학교 대학원

에너지시스템공학부

고 정 민

Electron Heat Transport Study in KSTAR L-mode Plasmas Using ECRH Modulation

KSTAR L-모드 플라즈마에서 ECRH 모듈레이션을 이용한 전자 열 수송 연구

지도 교수 나 용 수

이 논문을 공학석사 학위논문으로 제출함

2018년 2월

서울대학교 대학원

에너지시스템공학부

고 정 민

고정민의 공학석사 학위논문을 인준함

2018년 2월

위 원 장 함 택 수 (인)

부위원장 나 용 수 (인)

위 원 황 용 석 (인)

Abstract

Electron Heat Transport Study in KSTAR L-mode Plasmas using ECRH Modulation

Ko, JungMin
Department of Energy Systems Engineering
Seoul National University

In this study, we explore the electron heat transport in a simpler approach using a semi-empirical model, the so-called critical gradient model (CGM) that has not been applied to KSTAR before, instead of a complex theoretical approach. KSTAR experiments were designed to perform the perturbative analysis using electron cyclotron resonance heating (ECRH) modulation as well as power balance analysis. We determined the free-parameters of the semi-empirical model that can reproduce the experimental results by simulations using ASTRA. The ranges of free-parameters obtained through this process from KSTRA experiments are compared and analyzed with those obtained from other devices such as JET and ASDEX Upgrade. The dependences on the plasma parameters are conducted.

Keywords: electron heat transport, modulation, power balance analysis, perturbative analysis, ECRH (Electron cyclotron resonance

heating), electron heat flux, microturbulence, critical gradient model, KSTAR

Student Number: 2016-21285

Contents

List of Tables

List of Figures

Chapter 1

Introduction

1.1 Electron heat transport in tokamak plasmas

Exploring the energy transport has been an important topic in tokamak fusion plasmas because the transport properties are closely linked with the fusion plasma confinement and the design of future tokamaks. The electron heat transport has been widely studied for a couple of decades.

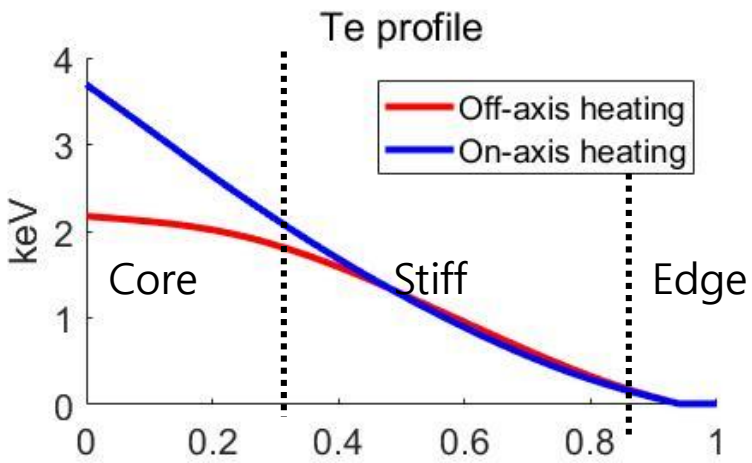

Figure 1.1 The division of the electron temperature profile into three regions affected by different mechanisms.

Previous researches have revealed that the electron temperature profile can be divided into three regions; the core, the edge, and the stiff region which is the region between them [1,2]. Unlike the core region, the stiff region of the profile is insensitive to an auxiliary heating like ECRH (Electron Cyclotron Resonance Heating) [3,4,5]. That is, when the $(\nabla T_e/T_e)$ exceeds the critical value $(\nabla \mathrm{T_e}/T_e)_c$ due to an external heating, the diffusivity χ_e rapidly increases so that the $(\nabla T_e/T_e)$ is lowered to maintain $(\nabla T_e/T_e)$ close to the threshold value. This property is called a "profile resilience" or "profile stiffness" [6].

These three regions are known to be influenced by different mechanisms. The core and the edge region are mainly affected by the MHD instability such as sawtooth and the radiation, respectively. In the stiff region, the tendency to maintain the marginally stable profile is considered as a result of microturbulence because the high value of the heat conductivity is beyond the neoclassical level [7,8]. In the electron channel, trapped electron mode (TEM) [9,10,11] and electron temperature gradient (ETG) mode [12,13] are good candidates to dominate the electron heat transport. Although these two types of microturbulence are generated by different mechanisms, they both exhibit a threshold value of $(\nabla T_e/T_e)$ and a stiffness value which appears when $(\nabla T_e/T_e)$ is beyond the threshold value that is in accordance with a "profile stiffness" property. Therefore, they can express the electron heat transport by characterizing a threshold and a stiffness. According to this idea, a model which can explain the electron heat diffusivity by its threshold and its stiffness is introduced in many other researches which will be described in the next chapter.

1.2 Critical Gradient Model

Electron transport is difficult to describe with a single mechanism as mentioned above. There are several models such as Weiland [10], IFS-PPPL [1], and GLF23 [14] for describing anomalous transport which is a main property in the stiff region. However, there have been observed some inconsistent results between these models. In addition, although these models are stringent, predicting and calculating with these models are delicate, and a simulation is a very computing resource- and time-consuming process. Thus, instead of using these first principle models, there have been numerous attempts to introduce simpler models which can mimic the tendency observed in the experiment such as the Critical Gradient Model (CGM) [15]. Experiments have shown that the electron diffusivity increases with increasing R/L_{T_e} in various devices [16] regardless of types of the dominant microturbulence. By modeling its threshold and stiffness analytically which have been observed in experiments, it becomes possible to represent the electron heat flux with a single global model.

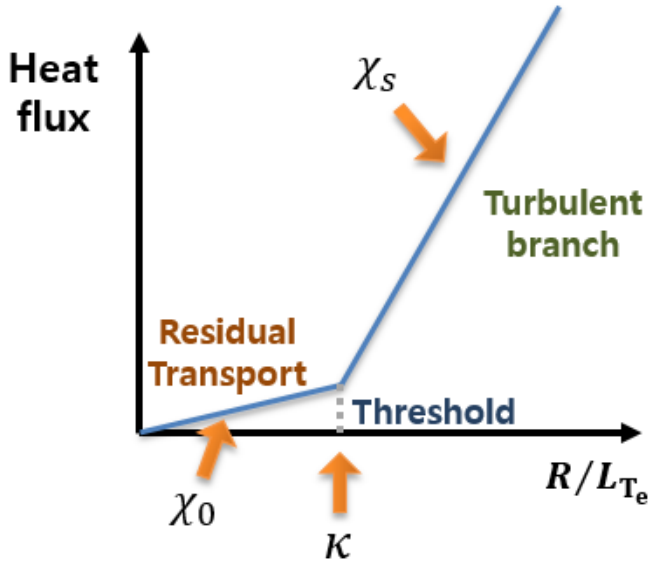

Figure 1.2 The general electron heat fluxes versus the electron temperature gradient length.

The semi-empirical CGM in [15] is expressed as

$$\chi_e = \chi_{GB}\left[\chi_S\left(\frac{R}{L_{T_e}} - \kappa\right)H\left(\frac{R}{L_{T_e}} - \kappa\right) + \chi_0\right]$$

Here, $H(x)$ is a Heaviside function which describes a step function with threshold κ. χ_0, χ_s, and κ are free-parameters which characterize the residual flux, the stiffness, and the threshold, respectively. Fig. 1.2 shows that the characteristics in the electron heat flux are distinguished based on the threshold value κ in $(\nabla T_e/T_e)$. When $(\nabla T_e/T_e)$ is over the threshold, the electron diffusivity increases with χ_s. Therefore, the electron temperature profile in the edge region which usually has higher value of $(\nabla T_e/T_e)$ due to the low electron temperature can be mainly described by the parameter χ_s. Similarly, in the core region which usually has low value of $(\nabla T_e/T_e)$, the electron profile and the transport properties are mainly explained by the parameter χ_0. In this paper, these parameters are assumed to be constant in all the regions for simplicity, though there might exist some radial dependencies due to the radially different plasma conditions. These parameters can change the transport properties so that they can also affect not only T_e but also the harmonics of amplitudes and phases when a modulation of the external heating source is applied. The propagation information of T_e variation according to the modulation will be used to determine the free-parameters χ_0, χ_s, and κ that reproduce experimental properties well.

CGM and its free-parameters can provide transport models exhibiting the characteristics of various plasma states and can be applied to the global confinement scaling [2]. Thus, we can compare the ranges of free-parameters

obtained from KSTAR results in multiple tokamak devices. In addition, since the free-parameters of CGM are directly affected by plasma parameters, global transport properties and their dependencies according to the plasma parameters such as the magnetic shear s can also be estimated.

The experimental results obtained from JET [17,18], ASDEX Upgrade [19,20], and TCV [21] showed that the electron transport can be expressed with CGM. Since there are no related experiments and appropriate data in KSTAR, a study such as designing experiments and testing the ranges of free-parameters in L-mode plasmas can be a good initial work for preparing more comprehensive exploration of electron transport in H-mode and ITB plasmas.

1.3 The analysis methods

There are two ways of deducing the diffusivity in the literature, and both the methodologies are adopted here. The first method is the power balance analysis, which calculates the heat flux and its diffusivity to create the electron temperature profile measured in the experiments given the input power of ohmic/ECRH power and the output power of radiation/collision etc. The second one is the perturbative analysis where the modulation of the ECRH power is applied to study the transient transport [17]. We can calculate the experimental diffusivity from the power balance method, and find the parameters for CGM modeling by the perturbative method applying the ECRH modulation. These methodologies will be explained in more detail in Chapter 3.

Since the power balance analysis alone cannot find the unique solution of

CGM [23], the solution is mainly determined by the perturbative analysis and the power balance results are used only for comparison. This is because there are many solutions that can satisfy the results obtained from the power balance analysis as shown in the figure below. Hence, through the perturbative analysis, we reduce the number of possible solutions.

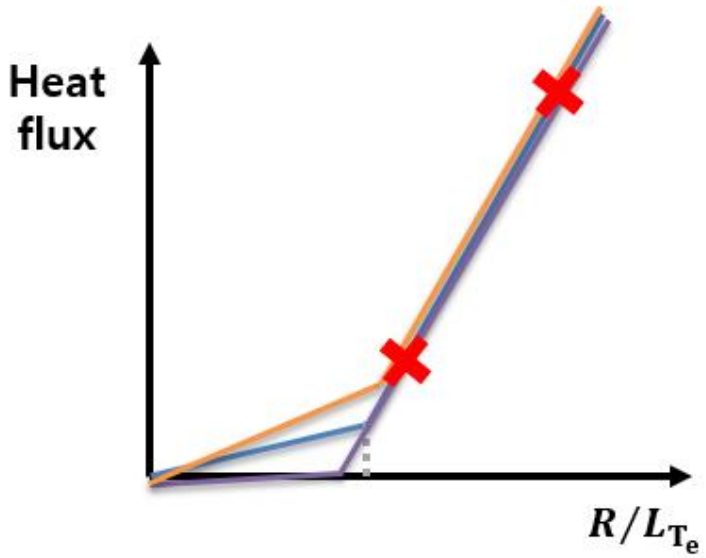

Figure 1.3 Several possible cases (orange, blue, and violet curve) obtained from the power balance analysis alone using CGM at the two points presented as cross.

1.4 Objectives and scope of this work

This work is to find the simplest empirical model which can simulate the main transport properties rather than to simulate some detailed physical phenomenon using theoretical models. This approach may provide much simpler picture to understand the electron heat transport and useful applications such as scaling and prediction. Physical insight can be obtained by comparison with other devices.

There are no applicable experiments in KSTAR with CGM, though there have been various related experiments in JET, ASDEX-Upgrade, and TCV. Hence, the first purpose of this study is to design perturbative experiments for electron transport study using ECRH heating source modulation in KSTAR L-mode plasmas. Conducting these experiments, we can explore the feasibility of CGM by using the power balance analysis and the perturbative analysis. The results will provide the ranges of three free-parameters χ_0, χ_s, and κ so that comparison with multiple devices is possible. These experiments will become an initial work for the further study of electron transport properties such as identifying the turbulence modes or exploring more complex H-mode/ITB plasmas. Lastly, we can study a possibility of specific plasma parameter dependences in CGM in the KSTAR tokamak. These results may be compared with the other observed dependences in other tokamak devices.

Chapter 2

Experimental Set-Up

In the electron heat transport study using the perturbative analysis, the modulation of the heating source such as ECRH is necessary. Previously, there were several ECRH modulation experiments in KSTAR L-mode plasmas, but full-transport simulations were difficult because there was no experiment using 70:30 duty cycle of the ECRH modulation which enables to obtain multiple harmonics amplitudes and phases of the T_e evolution. The propagation information from multiple harmonics can provide global transport characteristics and the more stringent validation of simulating transport properties.

Therefore, we planned modulation experiments to make the multiple harmonic analysis possible. Plasma parameters suitable for KSTAR are determined in these experiments considering the MHD instabilities and measurement of diverse diagnostics. The ECRH power is modulated as a heating source. The Fourier transformed response of the T_e modulation is analyzed more accurately by using the high resolution electron cyclotron emission (ECE) diagnostics of KSTAR. The transport simulation code and the methods of calculating configurations will be described in this chapter.

2.1 Plasma parameters

In this work, we use four L-mode discharges in the KSTAR tokamak (R = 1.8 m, a = 0.5 m) with D_2 plasmas: #18361, #18363, #18364, and #18365. In all these four discharges, the ECRH is modulated so that the sawteeth effect should be suppressed because the modulated electron temperature signal might be interrupted with the effect. Hence, the magnetic field B_T is kept to be high as 2.2 T and the plasma current I_P is kept to be low as 0.4 – 0.5 MA to apply high q_{95}. These differences lead to the variation of q_0, q_{95}, and the profile of the magnetic shear s. The value of Z_{eff} is assumed to be 2.0 in this study.

There have been several cases that the edge ECE signals are distorted when the line-averaged density is too low due to the suprathermal electrons. To prevent these distortions, the line-averaged electron density $n_{e,l}$ is feedback-controlled to be 2.0-2.5 m^{-3}.

	18361	18363	18364	18365
B_T (T)	2.2	2.2	2.2	2.4
I_P (MA)	0.5	0.4	0.4	0.4
$T_{e,0}$ (keV)	2.2	1.3	1.5	4
$n_{e,l}$ (m^{-3})	2.0	2.4	2.5	2.4
Z_{eff}	2.0	2.0	2.0	2.0
q_0	1.3	1.7	1.7	1.3
q_{95}	5.5	7	7	7.5

Table 2.1. The main plasma parameters in KSTAR #18361 and #18363-#18365 discharges.

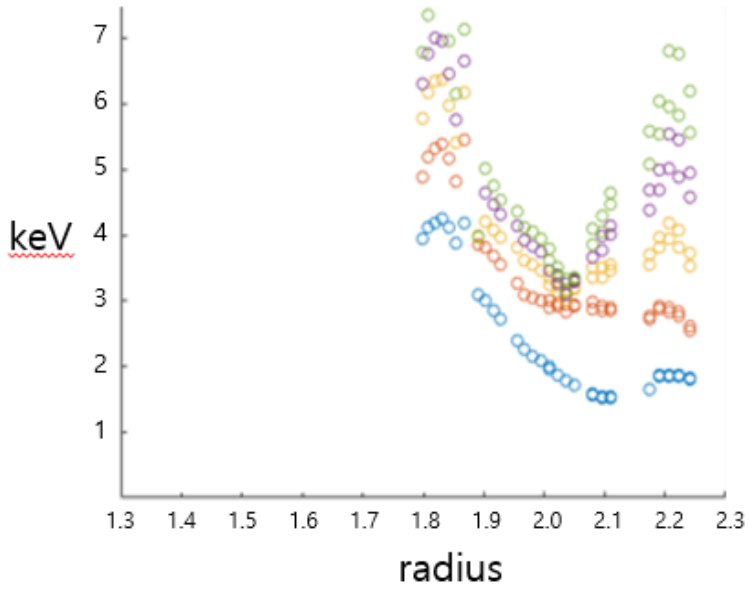

Figure 2.1 Distortion of the ECE diagnostics at the low line-averaged electron density due to suprathermal electrons.

2.2 Diagnostics & Measurements

In this work, we apply the perturbation in the heating source, i.e. ECRH and observe the propagation of the perturbation in the electron temperature T_e in each radial point. Hence, the accurate measurement of the electron temperature T_e is significantly important which is provided by the ECE diagnostic with the high resolutions as 0.01 ms in KSTAR. In addition, the ion temperature T_i was measured by the CES (charge exchange recombination spectroscopy) diagnostics. NBI (Neutral beam injection) blips are applied at every second in the plasma current flat-top phase for the CES measurement. The line-averaged electron density $n_{e,l}$ is measured by the interferometer. The electron density n_e profiles are obtained by the Thomson scattering diagnostics. The plasma equilibrium information such as q_{95} and κ_{elong} is obtained from RT-EFIT equilibrium calculations. However, for more realistic safety factor estimation, q-profiles are reconstructed using ASTRA by solving the current diffusion.

2.3 ECRH Settings

For the perturbative analysis on the electron temperature profiles in our experiments, ECRH plays a critical role and its settings are mostly important. A 140 GHz ECRH is applied with 0.8 MW of heating power in these experiments, changing the resonance location in every shot from on-axis ($\rho = 0.14$) to off-axis ($\rho = 0.41$) in order to obtain low and high values of heat flux

and the various electron temperature gradient R/L_{T_e} as similar as in [20]. #18361 and #18363-#18364 discharges are the off-axis heating shots, and #18365 discharge is the on-axis heating shot. During the current flat-top phase (1 – 10 s), the steady ECRH phases are sustained in 2.5 – 3.5 s and 7.5 – 8.5 s for the power balance analysis. Hence, two points are chosen for the power balance analysis at every discharges. The ECRH power is modulated at 3.5 – 7.5 s for the perturbative analysis.

	18361	18363	18364	18365
ECH Location	$\rho = 0.34$	$\rho = 0.38$	$\rho = 0.4$	$\rho = 0.1$
ECH Power (MW)	0.8	0.8	0.8	0.8

Table 2.2. The resonance location of ECRH and its injection power in KSTAR #18361 and #18363-#18365 discharges.

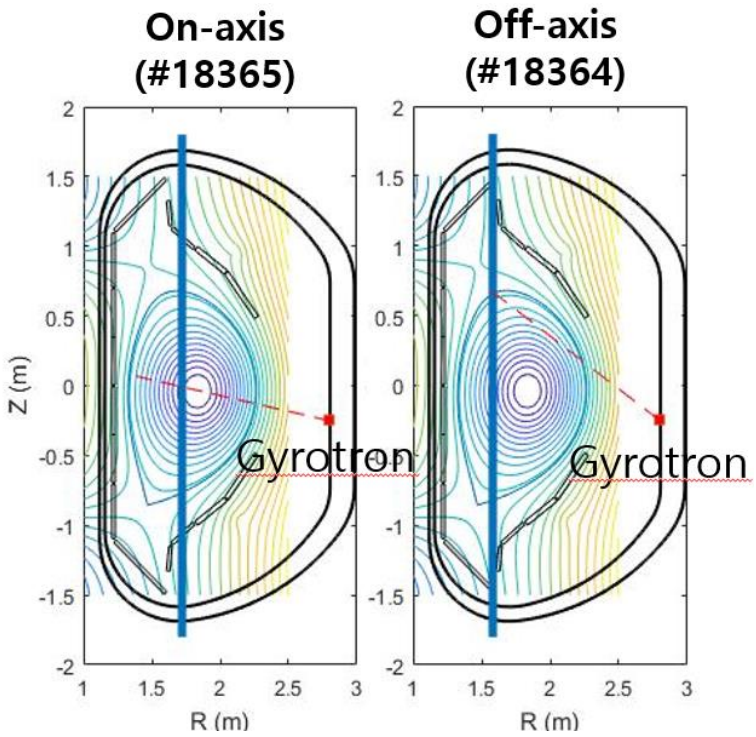

Figure 2.2 Schematic view of the ECRH injection trajectory in the on-axis heating discharge (#18365) and the off-axis discharges (#18361, #18363, and #18364).

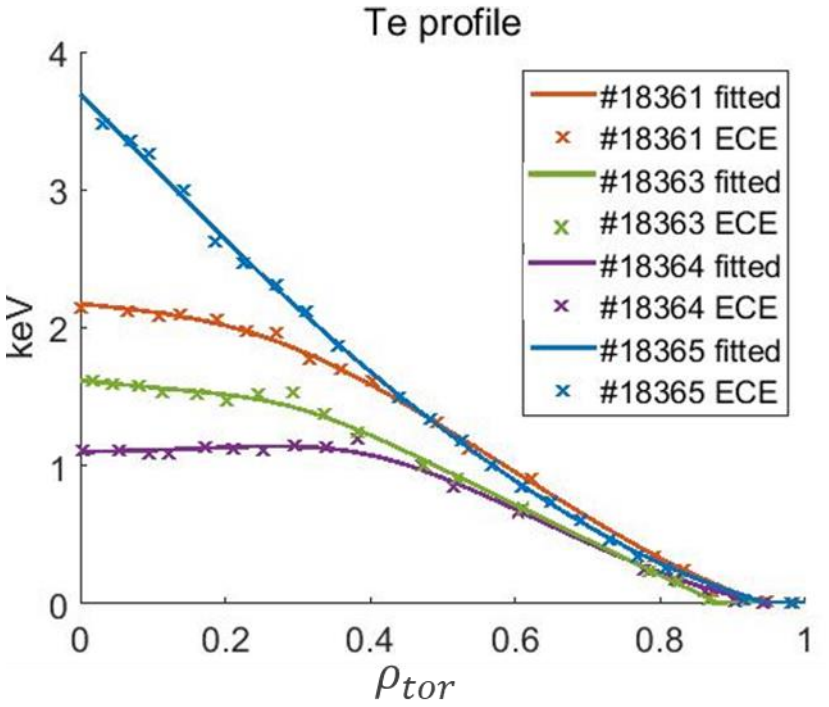

Figure 2.3 The electron temperature profiles in normalized radius (ρ_{tor}) for various ECRH deposition profiles. The T_e gradients vary with the ECRH resonance locations.

After several modulation frequencies were tested as 10, 20, and 30 Hz in #18361 and it was set to be 20 Hz which shows the clearest signal when it is Fourier transformed for #18363-#18365 discharges. The RF power is fully modulated, i.e., the value of $(maximum\ RF\ power - minimum\ RF\ power)$ is 100% of the maximum power, 0.8 MW. The RF power deposition profile and the absorption rate are calculated by the TORAY ray-tracing code in the simulation.

The duty cycle is set to be 7:3 as shown in Fig. 2.4 to obtain not only the fundamental harmonic amplitudes and phases of the temperature response, but also the higher harmonics such as the second harmonics. If we set the duty cycle as 5:5 as other usual experiments in KSTAR, the fundamental harmonics can be measured clearly but the amplitude of the second and the third harmonics is very small so that we cannot obviously analyze the higher harmonic responses. The second harmonic T_e responses are necessary to determine the unique solution of CGM free-parameters, and the third harmonic T_e responses may provide more stringent verification of the full transport simulation can be achieved so that we can show the CGM modelling simulates a more realistic transport properties. Hence, we tried to obtain the third harmonic Fourier transformed analysis of the T_e modulation response at the stage of designing the experiment. However, in reality, only the second harmonic result of modulation response could be obtained because of the ECE measurement noise. It might be better if we obtain the third harmonic T_e responses in the future, though there is no problem to calculate the solution of the free-parameters in CGM.

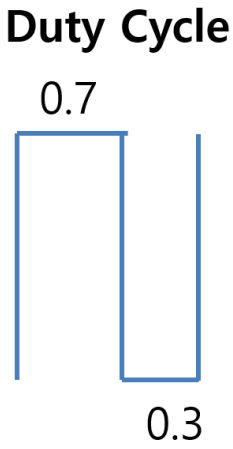

Figure 2.4 The waveform of the ECRH injection power with 7:3 duty cycle for the multiple harmonics of FFT (Fast Fourier Transform) of the electron temperature responses.

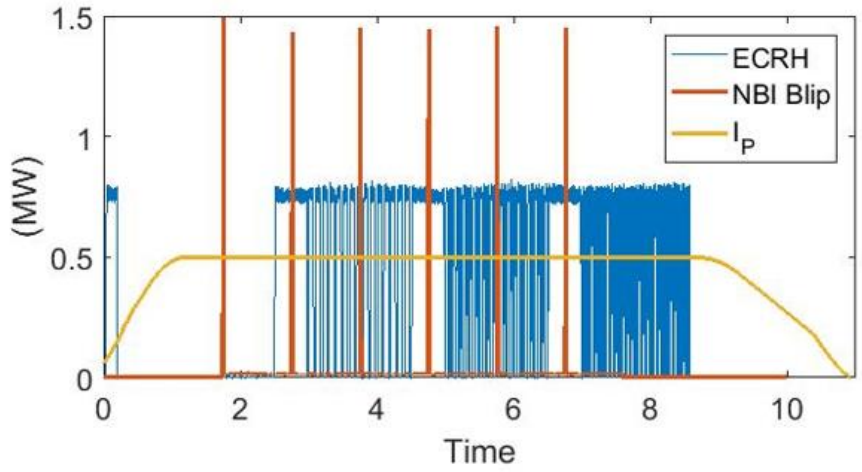

Figure 2.5 The shot traces of #18361 discharge in KSTAR. The NBI blips are injected for the measurements of T_i during the flat-tops. The ECRH power is modulated with 10 Hz in 3-4.5 s, 20 Hz in 5-6.5 s, and 30 Hz in 7-8.5 s.

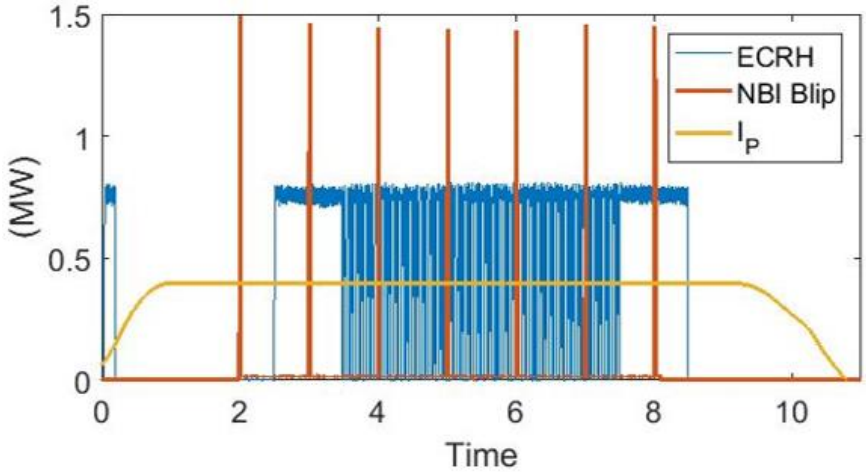

Figure 2.6 The shot traces of #18363-#18365 discharge in KSTAR. The NBI blips are injected for the measurements of T_i during the flat-tops. The ECRH power is modulated with 20 Hz which shows the clearest FFT signal in #18361.

Chapter 3

Analysis Methods

How the static analysis and the dynamic analysis are performed will be described in Chapter 3.1 and 2.3, respectively. The static method, i.e., the power balance analysis is used to calculate the electron heat transport and its diffusivity using the experimental measurements. However, the electron transport study using CGM cannot be fully determined by the power balance analysis alone. Therefore, we use the dynamic method together to provide further information such as the location of the heating source injection and the propagation information, so that we can optimize the free-parameters in the transport model using the information via simulation. Hence, the power balance method is used only to deduce the experimental electron heat fluxes in KSTAR.

The comparison between the simulation and the experiment can verify the feasibility of CGM in KSTAR. In addition, it will provide the ranges of free-parameters of CGM in KSTAR and their comparison with other tokamak devices. This chapter deals with the methodologies and the results of applying these methodologies will be described in the next chapter.

3.1 Power Balance Analysis

In steady-state plasmas, we can obtain the electron heat conductivity χ_e by the power balance method, which considers the input power and the output power. In this work, input power is ohmic power and RF power, and the output power is from the power exchange from electron to ion, radiation, and the collision with neutrals. In terms of the radiation power, the value of Z_{eff} is assumed to be 2.0 as mentioned above. Ignoring the convective term, the experimental χ_e obtained from the power balance analysis is

$$\chi_e = -\frac{q_e}{n_e \nabla T_e} \qquad (1)\ [22]$$

In our experiments, two steady ECRH phases in flat-top were used for power balance analysis in #18361 and #18363-#18365 and several points were chosen in each phase. In each point, the electron heat flux q_e is obtained in the transport simulation using the ASTRA code. The boundary position is set to be $\rho = 0.9$.

The static approach requires an exact calculation of input and output powers. To overcome the uncertainty from the assumption of Z_{eff} and calculation of the absorbed ECRH power, the perturbative analysis will be used to provide complementary information. In addition, the heat flux scan using the power balance alone in every radial points requires a complicated scaling process. Hence, these experimental values obtained from the power balance method will be used only to compare with the simulated values of heat fluxes by the modelling method using CGM.

3.2 Perturbative Analysis

In experiments, a modulation of the heating source can show how the perturbation propagates in plasmas while keeping other variables almost constant [23]. If we analyze the amplitude and the phase obtained from the Fourier transform, we can get the information of the propagation which can only be seen in the frequency domain. For example, the phase is minimum and the amplitude is maximum where the ECRH is injected. Similarly, plasma parameters affect the shape of the amplitude and the phase profiles. In case of our study, these information make the number of solutions reduced that are not unique with the power balance analysis alone.

Depending on the localization of the source, two types of approaches are possible for the perturbative experiments [17]. Among them, in this work, we use the second approach that enables the full transport simulation of the experiment, instead of the first approach which is a local calculation requiring a complex scaling in every radial points. The second approach uses a space- and time-dependent model for the heat diffusivity. In the transport simulation, free-parameters in CGM can affect the shape of amplitudes and phases. Therefore, by comparing the simulated amplitudes and phases with the actual experiments, we can obtain the best free-parameters which reproduce the experimental propagation information well.

For perturbative analysis, time evolutions of the experimental T_e are FFT

transformed at each radial point. Phase reference is set to the phase of the RF power. In each shot, LFS (Low Field Side) T_e profiles are chosen for the FFT analysis.

In the ASTRA simulation, the ECRH absorption power which is calculated by TORAY is integrated and modulated with 20 Hz as the experiments. Scanning χ_s, χ_0 and κ, the critical gradient model according to the free-parameters set is assigned to the electron diffusivity. The electron temperature responses in each radial points are FFT transformed, and these simulated results are compared to the experimental amplitudes and phases. Hence, 1st and 2nd harmonics measurements and the comparison with simulations are needed for a validation of full transport modelling.

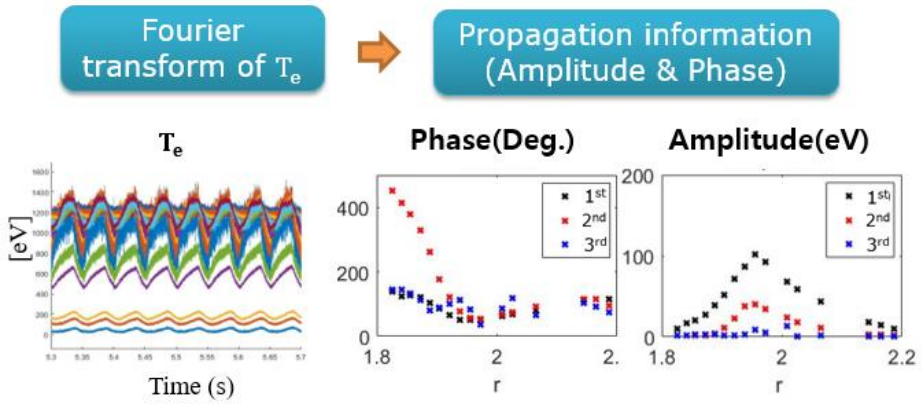

Figure 3.1 The electron temperature evolution and the Fourier transformed multiple harmonic phases and amplitudes. This propagation information will be compared to adjust CGM free-parameters.

Chapter 4

Results

To optimize the free-parameters in CGM, every different values for the free-parameters set are scanned within a wide range that covers the values obtained from various tokamak devices such as JET, ASDEX-Upgrade, and TCV. The different values calculated for each set show how much the simulation result using the ASTRA code differs from the actual KSTAR experimental value. We use the experimental values as multiple harmonics of the amplitudes and phases obtained from the perturbative analysis described in the previous chapter.

In Chapter 4.1, scanning method used in this work will be explained in detail and the scanning results will be presented. In Chapter 4.2, the difference-minimizing free-parameters obtained from the scanning result are shown. In addition, the predicted heat flux models from determined free-parameters will be described and compared with the experimental values in Chapter 4.2. The comparison with other devices will be addressed in Chapter 4.3. The possibility of the dependencies on the plasma parameter such as the magnetic shear will be discussed in Chapter 4.4.

4.1 Scanning Method

To adjust and optimize the free-parameters χ_0, χ_s, and κ_c that best reproduce the KSTAR experimental results, a scanning process is necessary. To set the ranges of scanning values, we refer to the previous studies in other devices [2], and set the ranges of χ_s, χ_0, κ as 0.01-3.01, 0.01-3.01, and 1-10, respectively which include all the ranges observed in other devices. The values of three free-parameters are scanned with the interval of 0.05, 0.05, and 1, respectively to figure out which value minimizes both the amplitude difference and the phase difference.

For each set of the free-parameters, the simulated amplitudes and phases profiles vary as shown in Fig. 4.1 and Fig. 4.2. The reason is that the transport properties deduced from the electron diffusivity with CGM vary according to the free-parameters in CGM. For example, the values of χ_0 mainly have an effect on the electron temperature profile in the core region. Similarly, the values of χ_s can change the shape of amplitudes and phases profiles in the stiff region. The values of κ usually determine the gradients of the electron temperature profile and the magnitude of the amplitude profiles. We will consider every effects of these parameters, and determine the most optimizing free-parameters in every discharges.

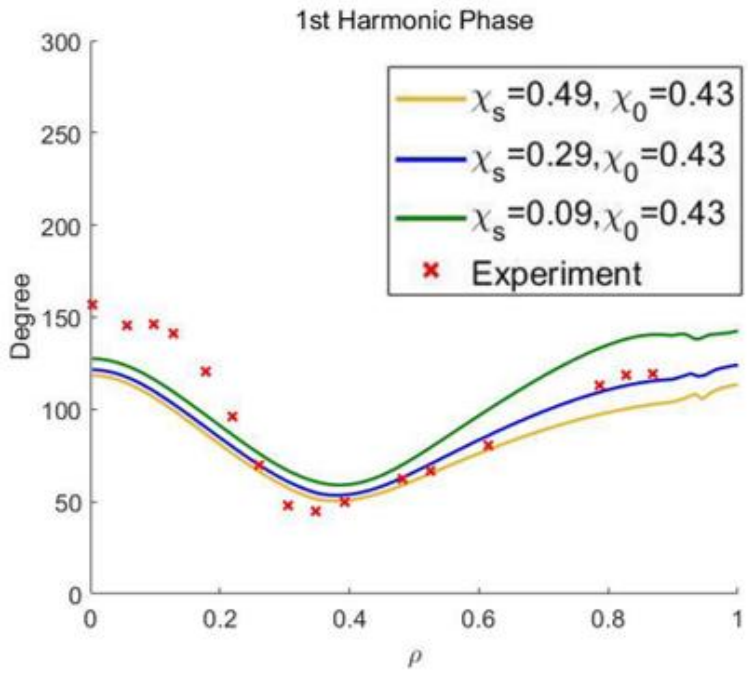

Figure 4.1 The first harmonic phase profile in normalized radius of #18364 (Off-axis). $\chi_s = 0.43$, $\chi_0 = 0.29$ (blue line) exhibits the best fit to the experiment (red cross).

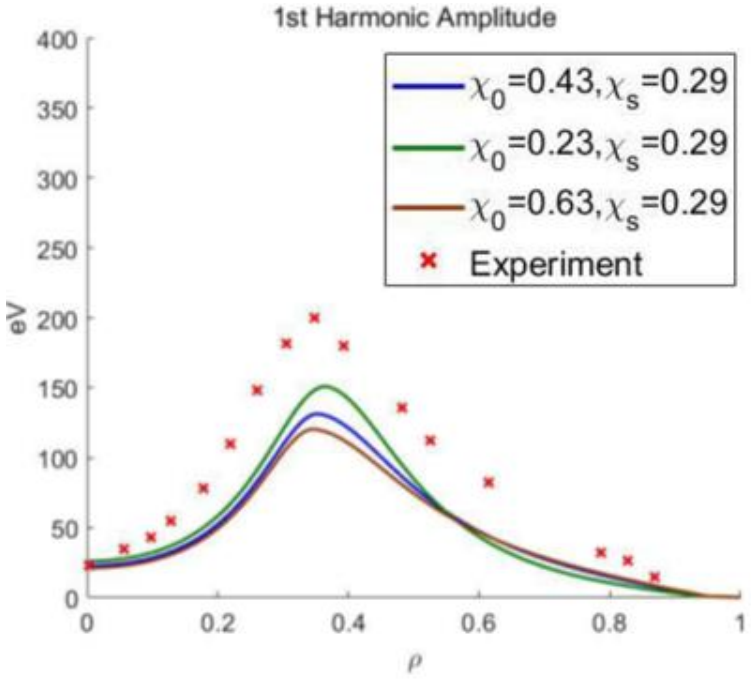

Figure 4.2 The 1st harmonic amplitude profile in normalized radius of #18364 (Off-axis). $\chi_s = 0.43$, $\chi_0 = 0.29$ (blue line) shows the best fit to the experiment (red cross). $\chi_s = 0.23$, $\chi_0 = 0.29$ (green line) is not selected due to the bigger phase difference.

Considering the turbulent regime, the differences were calculated as the average of the variation from the experimental values in the region of $\rho = 0 - 0.9$. Firstly, the differences in each parameter set were calculated by scanning χ_s and χ_0 with fixed κ. Then, the differences for each case are sorted in descending order in the amplitudes and the phases. If the parameter sets which minimize the difference values in each amplitude and phase are not in the intersection, the two parameter sets which minimize the differences in each group are compared. If there is no parameter set in the intersection, the next parameter set is considered until a parameter set appears in the intersection so that the selected parameter set can properly minimize the both 1st and 2nd harmonic amplitudes and phases. After χ_s and χ_0 are determined in this method, the differences in every κ were compared to determine κ.

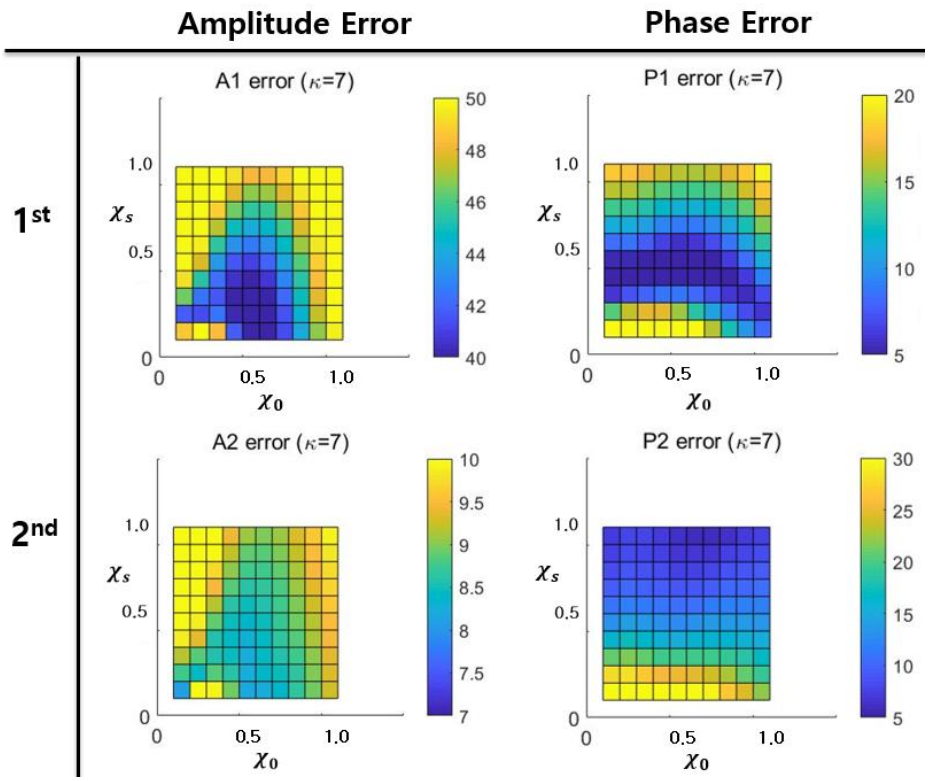

Figure 4.3 Differences plots in the first and the second harmonic amplitudes and phases. The blue color represents the small difference regions and the yellow color represents the larger difference regions. We can find χ_s and κ to minimize all differences in each case properly.

For example, the scanning process for #18365 discharge is described as following. The difference values are plotted in two-dimension according to χ_0 (*x*-axis) and χ_s (*y*-axis) as in fig. 4.3 with fixed κ as 7. In the 1st harmonic amplitude, the difference is minimized when χ_0 is around 0.6 and χ_s is around 0.3. Similarly, in the 1st harmonic phase, the difference is minimized when χ_s is around 0.4. Though there is no clear region which minimizes the differences in the 2nd harmonic phase, it still helps determine the parameter set since it suggests the larger value of χ_s should be chosen if the differences according to χ_s in the other amplitude and phase are not that different.

There always exists small level of differences in all phases and amplitudes even we optimized the free-parameters. It maybe due to the inaccuracy which is caused from the assumption that there are no radial dependencies in the free-parameters χ_s, χ_0 and κ. Furthermore, there are some diagnostic errors in measurements of the electron temperature and density profiles.

4.2 Electron heat fluxes in CGM

According to the above criterion and the scanning process, proper values of χ_0, χ_s, and κ_c that minimize difference values are determined in the four discharges as shown in Table 4.1. The values of χ_s are in the range of 0.21-0.31, and the values of χ_0 are in the range of 0.11-0.61. Especially, the values of κ vary significantly in #18365 which is an on-axis heating shot. These distributions seem to be caused by variation of the plasma parameters in each discharges.

	χ_s	χ_0	κ
18361	0.31	0.11	4
18363	0.21	0.61	3
18364	0.26	0.41	3
18365	0.31	0.41	7

Table 4.1. Free-parameters in CGM determined by the scanning methods.

With the determined free-parameters shown in Table 4.1, the electron heat fluxes predicted by CGM are plotted as dotted lines, and compared with the experimental values obtained by the power balance analysis as presented as circles in Fig. 5-7. The electron heat fluxes are normalized to the gyro-Bohm scale, $q_{e,GB} = q_e/(q^{1.5} n_e T_e^2 \rho_s / eBR^2)$ [18]. The predicted fluxes with CGM in the on-axis heating shot #18365 (red dotted line) considerably differs from

the other off-axis heating shots in $\rho = 0.4$ and $\rho = 0.5$. As the normalized radius ρ goes outside as $\rho = 0.6$, the gradient of T_e in the on-axis heating shot gets similar with the other discharges so that the gap from other lines decreases. Most importantly, the predictions from CGM determined from the perturbative analysis seem to be well-matched with the results from the power balance results on KSTAR.

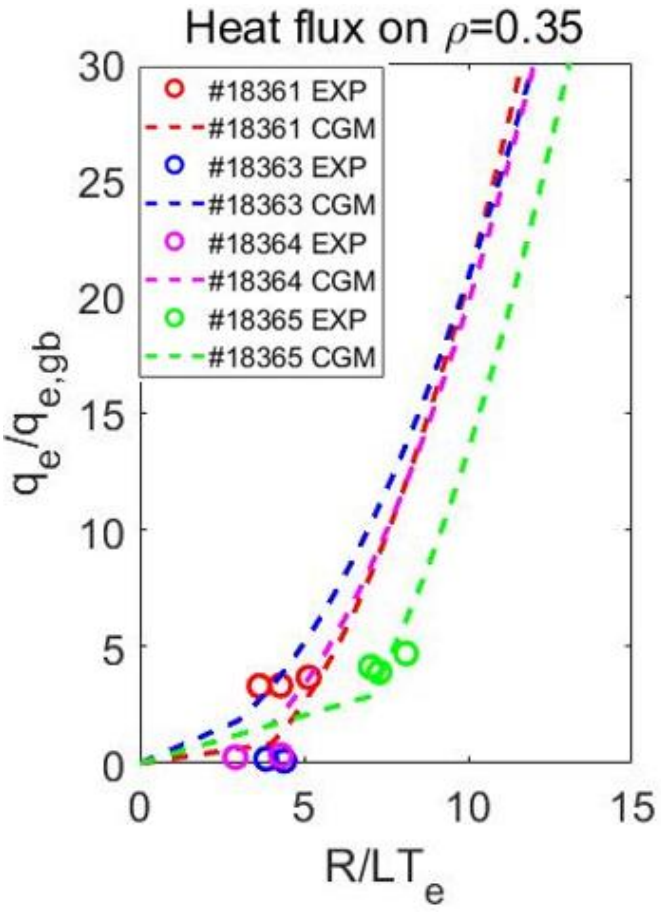

Figure 4.4 Gyro-Bohm scale normalized electron heat flux at $\rho = 0.35$. Dashed lines are CGM found in the perturbative analysis (Table 4.1). Circles are the experimental χ_e obtained from the power balance analysis.

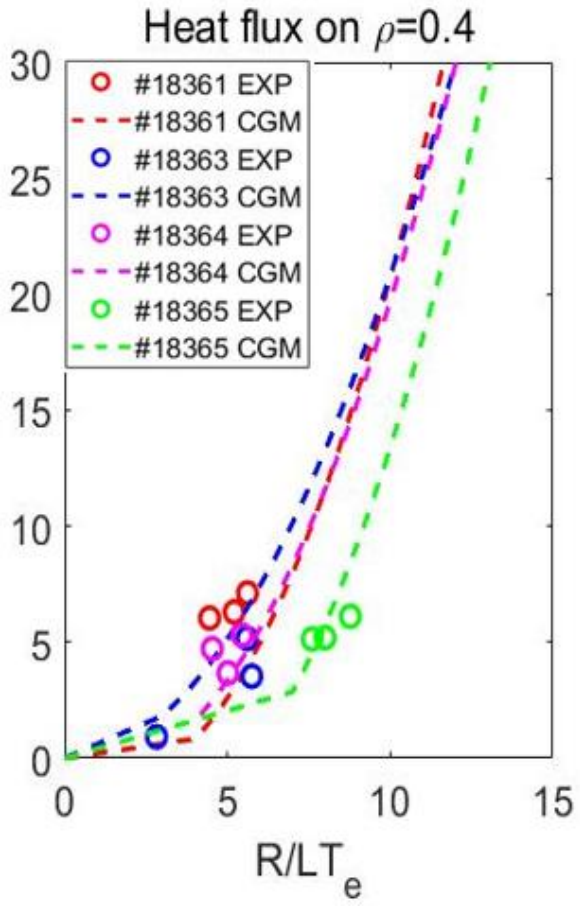

Figure 4.5 Gyro-Bohm scale normalized electron heat flux at $\rho = 0.4$. Dashed lines are CGM found in the perturbative analysis (Table 4.1). Circles are the experimental χ_e obtained from the power balance analysis.

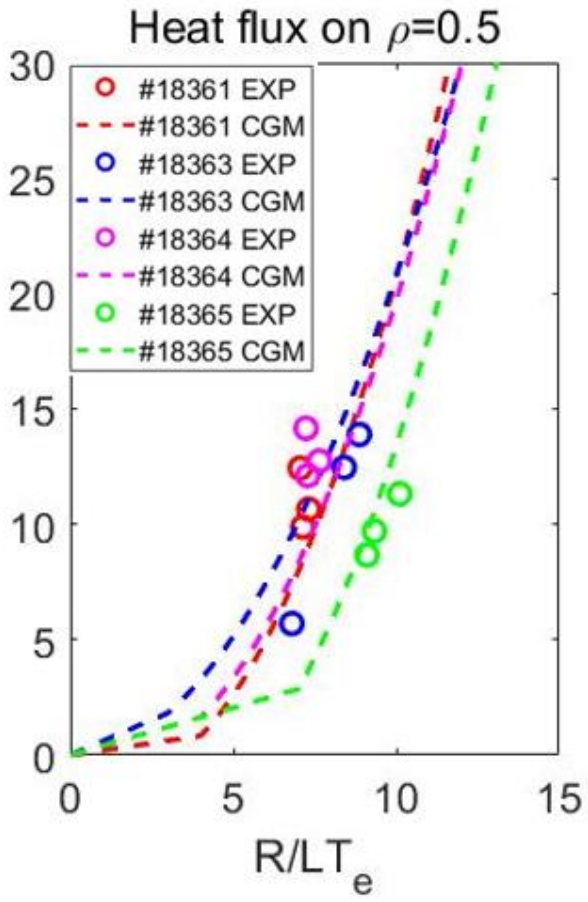

Figure 4.6 Gyro-Bohm scale normalized electron heat flux at $\rho = 0.5$. Dashed lines are CGM found in the perturbative analysis (Table 4.1). Circles are the experimental χ_e obtained from the power balance analysis.

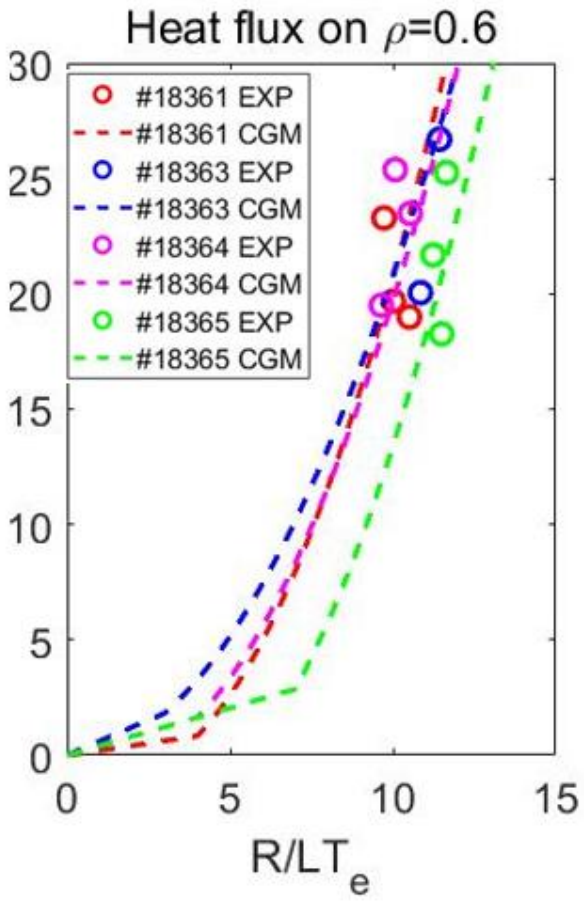

Figure 4.7 Gyro-Bohm scale normalized electron heat flux at $\rho = 0.6$. Dashed lines are CGM found in the perturbative analysis (Table 4.1). Circles are the experimental χ_e obtained from the power balance analysis.

4.3 Comparison of free-parameters in CGM

We can obtain the free-parameters in the CGM in #18361, #18363-#18365 L-mode shots in KSTAR using the scanning method. As explained in the previous sections, these free-parameters show the transport properties of the tokamak. For example, the stiffness χ_s shows how large the diffusivity increases when the gradient length R/L_{Te} is over the threshold value. The larger the value of χ_s is, the larger the heat transport becomes. Furthermore, the threshold κ shows how the microturbulence starts to grow from a certain gradient length. That is, the microturbulence is highly suppressed when the value of κ is high, and it can easily grow and become dominant when the value of κ is low. Using these free-parameters χ_s and κ obtained in KSTAR, we can compare the plasma properties between tokamak devices. The figure below [2] is a plot of χ_s and κ in JET, AUG (ASDEX Upgrade), FTU, and Tore-Supra where we added the results of KSTAR.

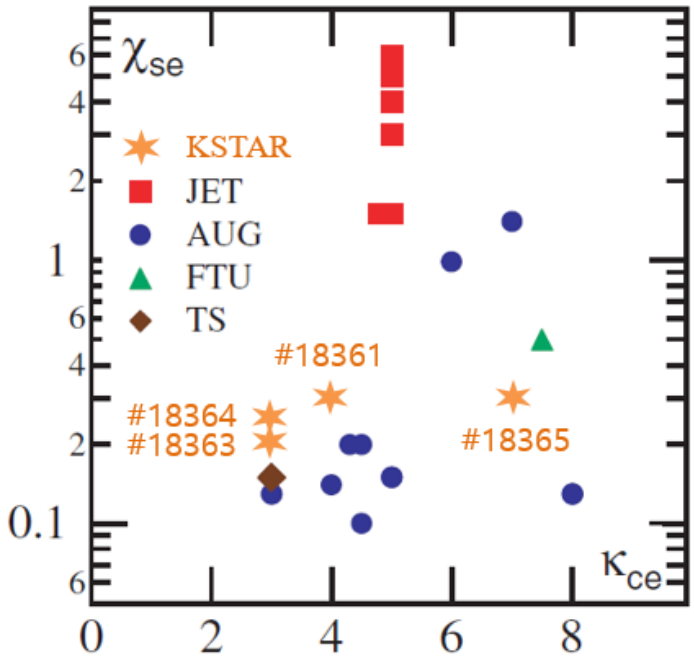

Figure 4.8 The stiffness χ_s and the threshold κ plot deduced in multiple tokamak devices shown in [2]. KSTAR results are added and plotted together.

As this figure shows, the values of stiffness χ_s in KSTAR are distributed in similar values to AUG, which are smaller than the values obtained from JET. In terms of the threshold κ, the values obtained in KSTAR is in the similar range of AUG. The sizes of the devices are considered to be the main reason for the difference in these values.

4.4 The dependences in CGM free-parameters on the plasma parameters

In the χ_s-κ plots in the previous section, we can observe the variation in the threshold κ in each shot in KSTAR. The value of κ in #18363 and #18364 is the minimum at 3, and the value of κ in #18365 is the maximum at 7. The difference in the values of the magnetic shear in these shots is thought to be a major candidate for the threshold variation.

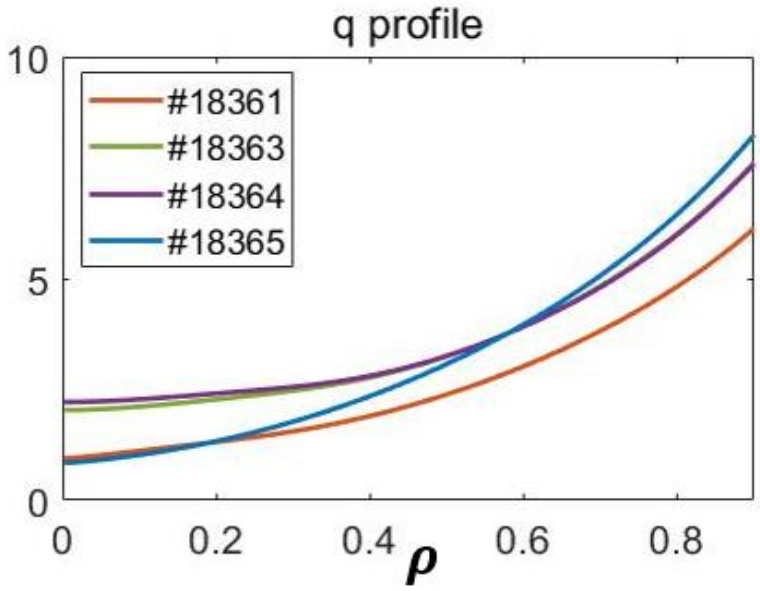

Figure 4.9 The q-profiles in KSTAR #18361 and #18363-#18365 discharges. These profiles are varied due to the difference of the plasma current I_P and the toroidal magnetic field B_T.

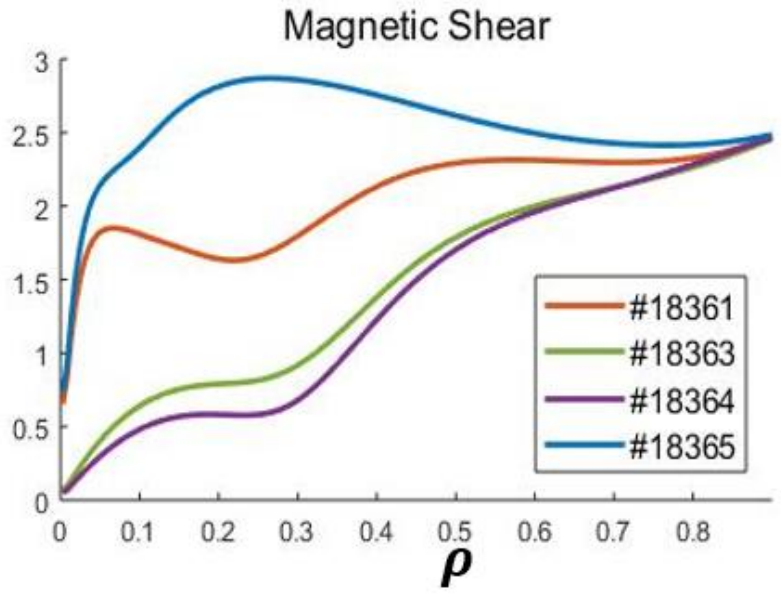

Figure 4.10 The magnetic shear profiles in KSTAR #18361 and #18363-#18365 discharges. These profiles are varied due to the difference of the plasma current I_P and the toroidal magnetic field B_T.

There have been many theoretical researches that indicated the magnetic shear may suppress the turbulent transport [24]. In addition, modulation experiments in JET also showed the correlation between the threshold κ and the magnetic shear [18]. In our cases, the safety factor q-profiles are plotted in the below figure, and the corresponding magnetic shear profiles are plotted in the next figure.

The magnetic shear difference is due to the variation of the plasma current I_P and the magnetic field B_T. The plasma current I_P is lowered to 0.4 MA in the discharges #18363-#18365 compared with #18361. Also, the magnetic field B_T increases in the #18365 discharge.

Chapter 5

Conclusion

ECRH modulation experiments and its perturbative analysis are conducted in KSTAR L-mode plasmas using the semi-empirical model CGM. This model allows to avoid a complicated theoretical calculation and a time-consuming simulation. In this work, we use 70:30 duty cycle in the modulation which enables the analysis using multiple harmonics T_e responses. We can apply this diffusivity model and the propagation information, the free-parameters in CGM are determined to best reproduce the experimental transport.

The optimizing process is made through a scanning method in ranges of 0.01-2.01 in χ_s and χ_0 and 1-10 in κ. After optimizing the free-parameters to reproduce the experimental amplitudes and phases, small differences are found between the experimental profiles and simulated results. The differences in the shape of phases and amplitudes are probably as a result of the radial dependencies of free-parameters which we assumed to be constant in this work. Applying a weighting or a parameter dependency might improve the model more realistically, but the simplicity of the model might be compromised.

Despite a small discrepancy in some regions, CGM reproduces the electron diffusivity quite well so that the feasibility of CGM in KSTAR is implied. The ranges of χ_s and χ_0, and κ are distributed in the similar range with ASDEX Upgrade. Especially, the experiment shows a possibility of the plasma parameter dependence of the electron heat diffusivity χ_e in KSTAR. There might be a few causes for the tendencies, but the magnetic shear is thought to

be one of the major reasons, as deduced in several theoretical researches and observed in modulation experiments in JET. If more experimental data is accumulated, further study can provide a clue for predicting the properties of the electron heat transport in KSTAR by using CGM.

These perturbative studies using CGM in KSTAR L-mode plasmas are meaningful because they can provide global feature of the electron transport in a simple form and become initial work for the further delicate transport studies. Considering the preliminary ranges of free-parameters found here, the perturbative experiments in KTSTAR H-mode/ITB discharges can be designed. In addition, the dependencies on plasma parameters such as T_e/T_i can be explored using the NBI power scanning, so that we may obtain a clue for identifying turbulence modes.

Bibliography

[1] M. Kotschenreuther, et al, "Quantitative predictions of tokamak energy confinement from first-principles simulations with kinetic effects", Physics of Plasmas, Vol. 2, No. 2381, 1995

[2] X. Garbet, et al, "Physics of transport in tokamaks.", Plasma Physics and Controlled Fusion, Vol. 46, No. 12, pp. B.557-B574, 2004

[3] R. Goldston, et al, Proc. 11th Int. Conf. on Plasma Physics and Controlled Nuclear Fusion Research (Kyoto,1986), Vol. 1 (Vienna: IAEA), pp 75, 1987

[4] F. Wagner, et al, “Experimental study of the principles governing tokamak transport.", Physical review letters, Vol. 56, No. 20, 1986

[5] T. C. Luce, C. C. Petty, and J. C. M. De Haas. "Inward energy transport in tokamak plasmas.", Physical review letters, Vol. 68, No. 1, 1992

[6] B. Coppi, "Nonclassical transport and the 'principle of profile consistency'"Comments, Plasma Physics and Controlled Fusion, Vol. 5, No. 6, 261-270, 1980

[7] F. Ryter, et al, Physical review letters, Vol. 86, No. 24, pp. 5498 – pp. 5501, 2001

[8] G. T. Hoang, et al, Physical review letters, Vol. 87, No. 12, 125001, 2001

[9] J. Weiland, et al, "Diffusive particle and heat pinch effects in toroidal plasmas", Nuclear Fusion, Vol. 29, No. 1810, 1989

[10] H. Nordman, et al, "Simulation of toroidal drift mode turbulence driven by temperature gradients and electron trapping", Nuclear Fusion, Vol. 30, No. 983, 1990

[11] J. Nilsson, et al, "On the collisionless trapped electron mode in fluid and kinetic descriptions", Nuclear Fusion, Vol. 35, No. 497, 1995

[12] F. Jenko, et al, "Electron temperature gradient driven turbulence",

Physics of Plasmas, Vol. 7, No. 1904, 2000

[13] W. Dorland, et al, "Electron temperature gradient turbulence", Physical Review Letters, Vol. 85, No. 5579, 2000

[14] R. E. Waltz, et al, "A gyro-Landau-fluid transport model", Physics of Plasmas, Vol. 4, No. 2482, 1997

[15] X. Garbet, et al, "Profile stiffness and global confinement.", Plasma physics and controlled fusion, Vol. 46, No. 9, pp. 1351-1373, 2004

[16] F. Ryter, et al, "Experimental study of trapped-electron-mode properties in tokamaks: threshold and stabilization by collision", Physical review letters, Vol. 95, No. 085001, 2005

[17] P. Mantica, et al, "Transient heat transport studies in JET conventional and advanced tokamak plasmas.", Proc. 19th Int. Conf. on Fusion Energy, 2002

[18] N. Bonanomi, et al, "Trapped electron mode driven electron heat transport in JET: experimental investigation and gyro-kinetic theory validation.", Nuclear Fusion, Vol. 55, No. 11, 113016, 2015

[19] F. Imbeaux, F. Ryter, and X. Garbet, "Modelling of ECH modulation experiments in ASDEX Upgrade with an empirical critical temperature gradient length transport model.", Plasma physics and controlled fusion, Vol. 43, No. 11, 1503, 2001

[20] F. Ryter, et al, "Electron heat transport in ASDEX Upgrade: experiment and modelling.", Nuclear fusion, Vol. 43, No. 11, 1396, 2003

[21] Y. Camenen, et al, "Electron heat transport studies under intense EC heating in TCV.", IAEA Technical Meeting on ECRH Physics and Technology for ITER (F1-TM-26015), Kloster Seeon, Germany, 2003

[22] B.J.D. Tubbing, et al, "Tokamak heat transport-a study of heat pulse propagation in JET", Nuclear Fusion, Vol. 27, No. 11, pp. 1843-1855

[23] N.J. Lopes. Cardozo, "Perturbative transport studies in fusion plasmas.", Plasma physics and controlled fusion, Vol. 37, No. 8, pp. 799.-852, 1995

[24] K. H. Burrell, et al, "Confinement phsics of H-mode discharges in DIII-D", Physics of Plasmas, Vol. 4, No. 1499, 1997

국문초록

이 연구에서는 복잡한 이론적 접근 대신 기존에 KSTAR 에 적용되지 않았던 경험적 모델을 도입하여 훨씬 더 간단한 접근법으로 전자 열 수송을 탐구한다. ECRH 모듈레이션을 이용하여 파워밸런스 및 섭동 분석 방법을 적용하여 실험 결과를 분석할 수 있도록 KSTAR 실험을 설계하였다. ASTRA 수송 코드를 사용하였고, 시뮬레이션 결과가 실험 결과를 가장 잘 재현할 수 있는 자유 매개 변수를 결정하였다. KSTRA 실험 분석을 통해 얻은 자유 매개 변수의 분포 범위를 JET 및 ASDEX Upgrade 와 같은 다른 장치에서 얻은 결과와 비교 분석하고, 자장전단을 중심으로 플라즈마 파라미터에 대한 의존성을 분석하였다.

주요어: 전자 열 수송, 모듈레이션, 파워밸런스 분석, 섭동 분석, ECRH (전자 사이클로트론 공명 가열), 전자 열속, 미소난류, 임계 구배 모델, KSTAR

학 번: 2016-21285